Ab Initio Computational Study of the Allenyl Cope Rearrangement of *syn*-7-Allenylnorbornene

James A. Duncan,* Joseph K. Azar,† J. Callan Beathe,† Scott R. Kennedy,† and Carolyn M. Wulf†

Contribution from the Department of Chemistry, Lewis & Clark College, Portland, Oregon 97219-7899

Received June 2, 1999. Revised Manuscript Received November 4, 1999

Abstract: Results of (8,8)CASPT2/6-31G*//(8,8)CASSCF/6-31G* level calculations on the potential surface for the conformationally restricted allenyl Cope rearrangement of *syn*-7-allenylnorbornene (**10**) to triene **11** are reported. The rearrangement is found to involve two separate transition structures **13** and **15**, the former 2.1 kcal/mol higher in enthalpy than the other, that both lead to a common diradical intermediate (**12**). These results differ substantially from those previously obtained for the allenyl Cope rearrangement of 1,2,6-heptatriene (**1**) to 3-methylene-1,5-hexadiene (**2**),[7] which has been shown to involve a single transition structure that either proceeds to diradical **3** or bypasses **3** to form **2** directly. The terminal methylene group of **10** is also shown to rotate in only one direction when passing through the lower-energy transition structure **13**, but appears to rotate freely in either direction when passing through **15**. This finding is shown to be remarkably consistent with the 90% stereoselectivity observed in the thermal Cope rearrangements of dimethyl allenylnorbornene derivatives racemic-**7a** and racemic-**7b**.[10] Furthermore, direct participation of the terminal allenyl π-bond is observed in the **10**→**11** rearrangement but not in the **1**→**2** rearrangement. This difference is evidenced by a comparison of the computed bond lengths and the calculated active space molecular orbitals in the two transition structures **13** and **15** verses transition structure **17**, the latter involved in the **1**→**2**/**3** pathways. Considering such evidence, it may be concluded that the particular restriction in conformational mobility afforded the 1,2,6-heptatriene moiety in **10** appears to force the participation of the terminal allenyl π-bond, resulting in an augmented Cope process.

Mechanisms of thermal Cope rearrangements have been the subject of numerous experimental and theoretical studies.[1] For example, (6/6)CASSCF calculations with a 3-21G basis set applied to the paradigmatic Cope rearrangement of 1,5-hexadiene yielded a single stationary state of C_{2h} symmetry corresponding to the transition state of a concerted pericyclic reaction.[2] However, when the basis set was improved to 6-31G* a potential energy surface (PES) with both a concerted and a nonconcerted pathway, involving a diradicaloid intermediate, was found.[3] Subsequently, the inclusion of dynamic electron correlation, using either CASPT2[4] or CASMP2[5] versions of multi-reference perturbation theory, showed that the Cope rearrangement of 1,5-hexadiene proceeds only by way of the concerted reaction.[6]

On the other hand, calculations and experimental investigations on the parent *allenyl* Cope rearrangement of 1,2,6-heptatriene (**1**) to 3-methylene-1,5-hexadiene (**2**) suggest that this rearrangement occurs by two different pathways that diverge after passage through a common transition state.[7] A calculation in which geometries were optimized at the (8,8)CASSCF level with the 6-31G* basis set and energies at these geometries derived from single-point calculations using dynamic electron correlation at the (8,8)CASPT2/6-31G* level located allylic diradical intermediate **3** and transition structures **17** and **18** (cf. Figure 2) connecting it to **1** and **2**, respectively. When the geometries of intermediate points were constrained to prevent allylic conjugation, a pathway from **17** to **18** was found along which the energy decreased monotonically. The existence of a second pathway from **1** to **2**, that bypasses diradical **3**, is consistent with experimental results obtained by Roth and coworkers[8] which have shown that approximately half of this rearrangement proceeds without formation of a trappable intermediate. Furthermore, these results are consistent with the stereochemistry observed by Berson and Wessel[9] for the pyrolysis of (*R*,*E*)-5-methyl-1,2,6-octatriene (**4**), an optically active dimethyl derivative of **1**. They concluded that at least 16% of the rearrangement, which affords all four possible stereoisomers of 4-methyl-3-methylene-1,5-heptadiene (**5**), passes through cyclohexane-1,4-diyl diradicals (**6**). The authors attributed this degree of stereoselectivity to two competitive chairlike pathways involving different conformations of **6**.

We have been exploring the mechanisms of the allenyl Cope rearrangements of *syn*-7-allenylnorbornenes experimentally for

† Lewis & Clark College undergraduate students.

(1) (a) Borden, W. T.; Loncharich, R. J.; Houk, K. N. *Annu. Rev. Phys. Chem.* **1988**, *39*, 213. (b) Houk, K. N.; Li, Y.; Evanseck, J. D. *Angew. Chem., Int. Ed. Engl.* **1992**, *31*, 682. (c) Houk, K. N.; Gonzalez, J.; Li, Y. *Acc. Chem. Res.* **1995**, *28*, 81.

(2) (a) Osamura, Y.; Kato, S.; Morokuma, K.; Feller, D.; Davidson, E. R.; Borden, W. T. *J. Am. Chem. Soc.* **1984**, *106*, 3362. (b) Morokuma, K.; Borden, W. T.; Hrovat, D. A. *J. Am. Chem. Soc.* **1988**, *110*, 4474.

(3) Dupuis, M.; Murray, C.; Davidson, E. R. *J. Am. Chem. Soc.* **1991**, *113*, 9756.

(4) Andersson, K.; Malmqvist, P. -Å.; Roos, B. O. *J. Chem. Phys.* **1992**, *96*, 1218.

(5) Kozlowski, P. M.; Davidson, E. R. *J. Chem. Phys.* **1994**, *100*, 3672.

(6) (a) Hrovat, D. A.; Morokuma, K.; Borden, W. T. *J. Am. Chem. Soc.* **1994**, *116*, 1072. (b) Kozlowski, P. M.; Dupuis, M.; Davidson, E. R. *J. Am. Chem. Soc.* **1995**, *117*, 774.

(7) Hrovat, D. A.; Duncan, J. A.; Borden, W. T. *J. Am. Chem. Soc.* **1999**, *121*, 169.

(8) Roth, W. R.; Wollweber, D.; Offerhaus, R.; Rekowski, V.; Lennartz, H−W.; Sustmann, R.; Müller, W. *Chem. Ber.* **1993**, *126*, 2701.

(9) Wessel, T. E.; Berson, J. A. *J. Am. Chem. Soc.* **1994**, *116*, 495.

10.1021/ja991838t CCC: $18.00
Published on Web 12/14/1999

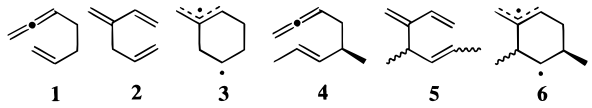

1 **2** **3** **4** **5** **6**

the past several years.[10] For example, the thermal rearrangement of racemic **7a** and **7b** have each been shown to separately

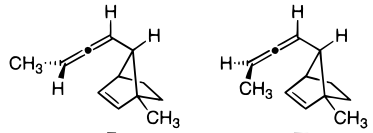

7a **7b**

rearrange to a mixture of the four trienes (*E*)-**8**, (*Z*)-**8**, (*E*)-**9**, and (*Z*)-**9**.[10d]

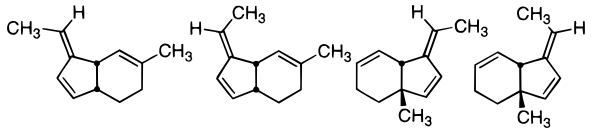

(*E*)-**8** (*Z*)-**8** (*E*)-**9** (*Z*)-**9**

Both reactions were found to be approximately 90% stereoselective. The rearrangement of epimer **7a** gave 95% of a mixture of (*E*)-**8** and (*Z*)-**9**, the products predicted by the Woodward−Hoffmann rules for (concerted) pericyclic reactions,[11] and 5% of a mixture of (*Z*)-**8** and (*E*)-**9**. Correspondingly, the rearrangement of the other epimer **7b** gave 96% of a mixture of (*Z*)-**8** and (*E*)-**9** and 4% of a mixture of (*E*)-**8** and (*Z*)-**9**. We have suggested[10] that at least some of the products may arise from tricyclic diradical intermediates.

Although none of the Cope rearrangements of **7a**, **7b**, and **4** are 100% stereoselective, the separate rearrangements of **7a** and **7b** are much more stereoselective (90%) than the rearrangement of **4** (68%).[9] This difference may be related to the greater restricted conformational mobility exhibited in **7a** and **7b** than in **4**, due to the presence of the rigid norbornene ring. In fact, *syn*-7-vinylnorbornene does not thermally undergo a Cope rearrangement but only decomposes when pyrolyzed.[10]

As can be seen clearly from the orbital representation of *syn*-7-vinylnorbornene in Figure 1a, the ends of the π-systems are not ideally placed for overlap, as compared to their placement in Cope rearrangements that may proceed through either a normal chair or boat transition state such as in the rearrangement of 1,5-hexadiene (cf. Figure 1b). However, as shown in Figure 1c, the rearrangement of **7a** (and **7b**) could take advantage of the terminal allenyl π-bond which can readily overlap with the π-bond in the norbornene ring to afford an augmented Cope process.

To further examine the role of the terminal allenyl π-bond in the Cope rearrangement of a conformationally restricted system, we have undertaken a computational study of the Cope rearrangement of *syn*-7-allenylnorbornene (**10**)[12] to triene **11** (cf. Figure 2).

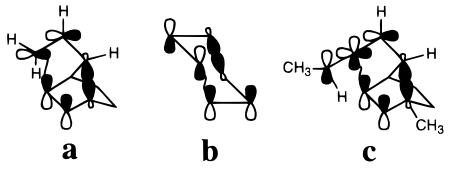

a **b** **c**

Figure 1. Active space orbital representations for Cope rearrangements: (a) Poor orbital overlap in *syn*-7-vinylnorbornene due to limited conformational mobility; (b) optimal overlap in the chair-form conformation for 1,5-hexadiene; (c) augmented Cope process involving the terminal allenyl π-bond in **7a**.

Computational Methodology

CASSCF calculations on all stationary points (**10**−**16**, Figure 2) were performed using an active space consisting of eight electrons in eight orbitals. The orbitals consisted of the four σ and π bonding orbitals and their antibonding counterparts. (8,8)CASSCF vibrational analyses were carried out, through numerical frequency calculations, to characterize stationary points as energy minima (**10**−**12** and **16**) or transition states (**13**−**15**) and to obtain zero-point energy differences. All CASSCF calculations made use of the Gaussian 94 suite of programs.[13]

The effects of dynamic electron correlation were included by performing single-point (8,8)CASPT2 calculations at all stationary points using MOLCAS 4.[14] The 6-31G* basis set was used for both the CASSCF and CASPT2 calculations. Three-dimensional structural representations of optimized geometries for structures **10**−**16**, prepared using MacMolPlt,[15] are shown in Figure 2. (Optimized structures **17** and **18**, also shown in Figure 2, were obtained in an earlier study.[7]) Transition vectors, obtained from the (8,8)CASSCF/6-31G* Gaussian 94 numerical frequency analyses, are also shown for transition structures **13**, **14**, **15**, **17**, and **18**. Molecular orbitals were visualized using Spartan,[16] which was also used to prepare Figure 6. Calculated carbon−carbon bond lengths for all structures in Figure 2 (**10**−**18**) are assembled in Table 1.

Results and Discussion

Structures **10**, **11**, and diradical intermediate **12** (Figure 2) were successfully optimized at the (8,8)CASSCF/6-31G* level with the correct active space orbitals in each case. In addition, transition structure **13**, linking **10** and **12**, as well as transition structure **14**, linking **11** and **12**, were located on the PES, as confirmed by the motions of their transition vectors (cf. Figure 2) and intrinsic reaction coordinate (IRC) calculations. The computed differences between the zero-point corrected enthalpies of **10**−**14** at the (8,8)CASPT2/6-31G*//(8,8)CASSCF/6-31G* level are shown in Figure 3a. The **10**→**13**→**12**→**14**→**11** pathway appears to proceed only with rotation about the C_1-C_2 bond such that the $H_aC_1H_b$ group rotates as shown in Figure

(10) (a) Duncan, J. A.; Bohle, D. B.; Blanchard, C. A.; Bossé, M. L.; Noland, T. W.; Ford, C. M.; Powell, M. A.; Sutton, M. C.; Eggleston, A. C.; Klevit, R. E.; Krueger, S. M. *J. Am. Chem. Soc.* **1982**, *104*, 2837. (b) Duncan, J. A.; Lee, B. A.; Teng, D. *J. Org. Chem.* **1983**, *48*, 1772. (c) Duncan, J. A.; Aki, L. Y.; Absalon, M. J.; Kwong, K. S.; Hendricks, R. T. *J. Org. Chem.* **1988**, *53*, 196. (d) Duncan, J. A.; Hendricks, R. T.; Kwong, K. S. *J. Am. Chem. Soc.* **1990**, *112*, 8433. (e) Duncan, J. A. *J. Org. Chem.* **1996**, *61*, 4455.

(11) Woodward, R. B.; Hoffmann, R. *The Conservation of Orbital Symmetry*; Verlag Chemie: Weinheim, Germany, and Academic Press: New York, 1970.

(12) Modeling the unsubstituted **10**→**11** case is less expensive computationally than modeling the dimethyl-substituted **7**→**8** + **9** case. Moreover, the methyl groups in **7** may serve primarily as stereochemical markers, having little, if any, influence on the mechanism of the rearrangement.

(13) Frisch, M. J.; Trucks, G. W.; Schlegel, H. B.; Gill, P. M. W.; Johnson, B. G.; Robb, M. A.; Cheeseman, J. R.; Keith, T.; Petersson, G. A.; Montgomery, J. A.; Raghavachari, K.; Al-Laham, M. A.; Zakrzewski, V. G.; Ortiz, J. V.; Foresman, J. B.; Cioslowski, J.; Stefanov, B. B.; Nanayakkara, A.; Challacombe, M.; Peng, C. Y.; Ayala, P. Y.; Chen, W.; Wong, M. W.; Andres, J. L.; Replogle, E. S.; Gomperts, R.; Martin, R. L.; Fox, D. J.; Binkley, J. S.; Defrees, D. J.; Baker, J.; Stewart, J. P.; Head-Gordon, M.; Gonzalez, C.; Pople, J. A. *Gaussian 94*, revision D.4; Gaussian, Inc.: Pittsburgh, PA, 1995.

(14) Andersson, K.; Blomberg, M. R. A.; Fülscher, M. P.; Karlström, G.; Lindh, R.; Malmqvist, P.-Å.; Neogrády, P.; Olsen, J.; Roos, B. O.; Sadlej, A. J.; Schütz, M.; Seijo, L.; Serrano-Andrés, L.; Siegbahn, P. E. M.; Widmark, P.-O. *MOLCAS*, version 4; University of Lund: Lund, Sweden, 1997.

(15) Bode, B. M.; Gorgon, M. S. *J. Mol. Graphics Mod.* **1998**, *16*, 133.

(16) *SPARTAN*, Version 5.0, Wavefunction, Inc. 18401 Von Karman Avenue, Suite 370, Irvine, CA 92715.

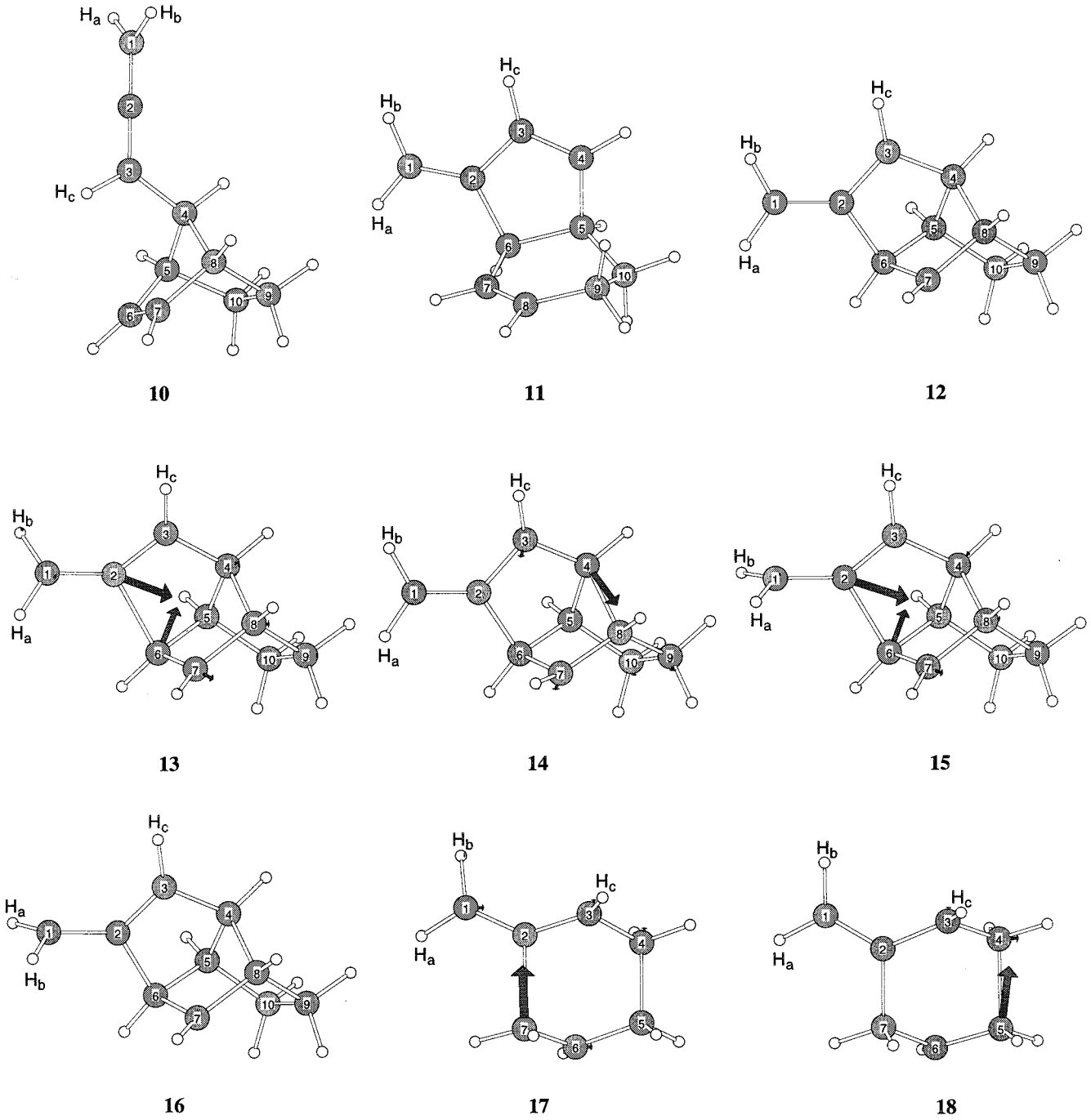

Figure 2. (8,8)CASSCF/6-31G* optimized geometries for **10**−**18**. Transition vectors are shown for transition structures **13**, **14**, **15**, **17,** and **18**. $H_bC_1C_3H_c$ dihedral angles in **12**−**18** are 3.5°, 57.3°, 19.3°, 88.4°, 87.4°, 78.2°, and 76.0°, respectively. Structures **10**−**12** and **16** were frequency characterized as minima. Imaginary frequencies for transition structures **13**, **14**, and **15**, were found to be −851, −801, and −763 cm^{-1}, respectively. (Transition structures **17** and **18** were characterized previously with imaginary frequencies of −727 and −687 cm^{-1}, respectively.[7])

3a;[17] a (8,8)CASSCF/6-31G* transition structure consistent with rotation in the opposite sense (i.e., **10**→**12** with H_a and H_b interchanged in **12** in Figure 3a), could not be located. This stereospecificity is also shown by the three-dimensional structural representations in Figure 4: The IRC beginning from transition structure **13** proceeds as far as structures **19** and **20**, which were readily optimized to **10** and **12** respectively.

In addition to transition structures **13** and **14**, we found transition structure **15** (cf. Figures 2 and 3b) on the (8,8)-CASSCF/6-31G* PES. It has a (8,8)CASPT2/6-31G* enthalpy 32.7 kcal/mol above that for **10** with a large $H_bC_1C_3H_c$ dihedral angle of 88.4°. (8,8)CASSCF/6-31G* IRC calculations have demonstrated that **15** connects to **10**. On the other side of transition structure **15**, the last structure obtained on the IRC path could be optimized to minimum structure **16** (cf. Figure 2) that resembles diradical **12** but without allylic stabilization ($H_bC_1C_3H_c$ dihedral angle = 87.4°). The results are shown by three-dimensional structural representations in Figure 5: In ascending the reaction coordinate from **10** to transition structure **15**, little if any rotation of the terminal methylene group (i.e., the $H_aC_1H_b$ group) is observed. Furthermore, Figure 5 shows clearly that the $H_aC_1H_b$ group continues to experience little

(17) Not only is this direction of rotation consistent with the Woodward−Hoffmann rules for pericyclic reactions,[11] but it is also clearly the direction which results in less framework distortion.

Table 1. Carbon−Carbon Bond Lengths (Å) for the Stationary Points on the (8,8)CASSCF Potential Surface for the Cope Rearrangement of *syn*-7-Allenylnorbornene (**10**) to Triene **11** (**10**−**16**) and the Transition Structures (**17** and **18**) for the Cope Rearrangement of 1,2,6-heptatriene (**1**), Obtained with the 6-31G* Basis Set

structure	C_1-C_2	C_2-C_3	C_3-C_4	C_4-C_5	C_5-C_6	C_6-C_7	C_7-C_8	C_8-C_9	C_9-C_{10}	C_5-C_{10}	C_4-C_8	C_2-C_6
10	1.32	1.32	1.51	1.55	1.52	1.34	1.52	1.55	1.56	1.55	1.58	
11	1.34	1.47	1.34	1.52	1.55	1.51	1.34	1.51	1.53	1.53		1.56
12	1.37	1.41	1.50	1.55	1.55	1.52	1.52	1.54	1.55	1.54	1.61	1.57
13	1.37	1.36	1.49	1.54	1.54	1.43	1.50	1.55	1.55	1.54	1.63	1.90
14	1.36	1.43	1.44	1.54	1.55	1.52	1.46	1.53	1.54	1.53	1.90	1.58
15	1.41	1.34	1.51	1.54	1.54	1.44	1.51	1.54	1.56	1.54	1.60	1.84
16	1.46	1.34	1.51	1.54	1.55	1.50	1.52	1.54	1.55	1.54	1.60	1.60
17	1.34	1.40	1.48	1.65	1.47	1.41	1.92					
18	1.34	1.47	1.43	1.84	1.43	1.48	1.61					

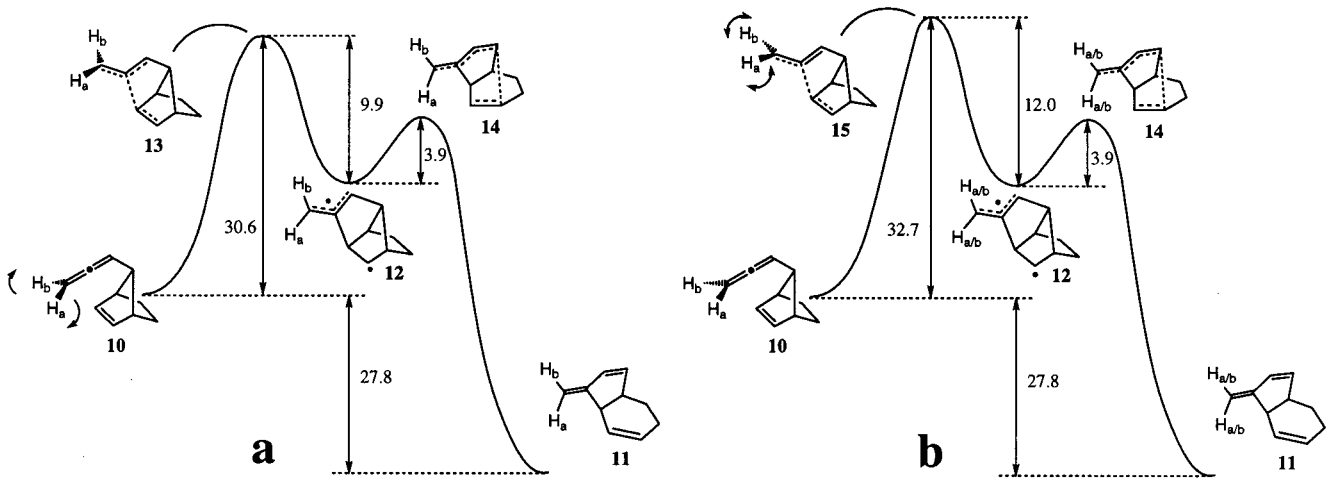

Figure 3. Reaction coordinate diagram showing zero-point corrected enthalpy differences (in kcal/mol) among optimized structures **10**−**15**, computed at the (8,8)CASPT2/6-31G*//(8,8)CASSCF/6-31G* level of theory: (a) "stereoselective" **10**→**11** process; (b) "nonstereoselective" **10**→**11** process.

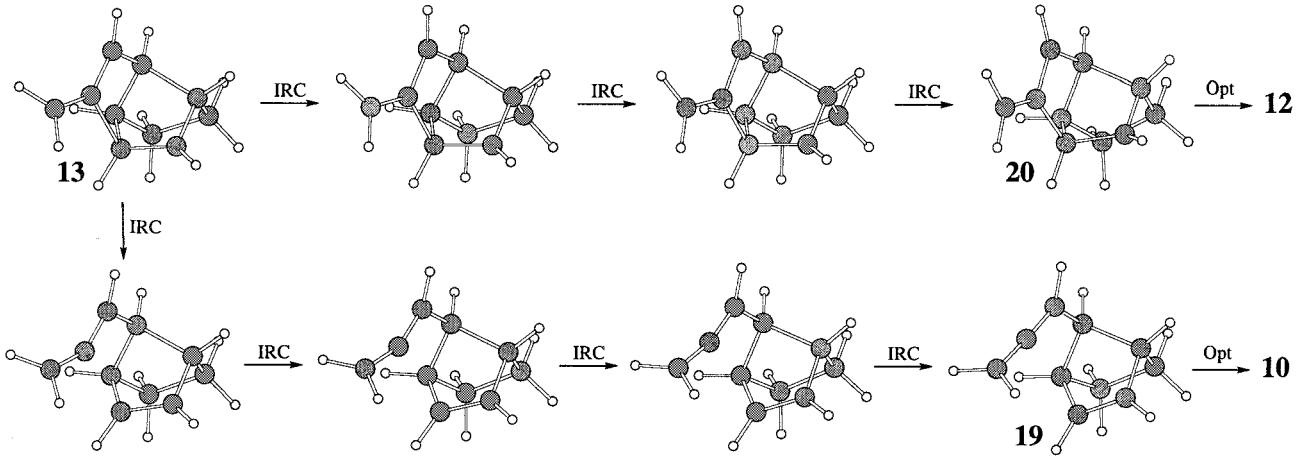

Figure 4. IRC structures for the rearrangement of **10** to **12**, involving transition structure **13**. Structures **19** and **20** represent the final points that could be obtained, on either side of the transition structure, by the IRC method. Intermediate IRC structures (i.e., unnumbered ones) represent equally spaced points between **13** and **19** as well as between **13** and **20**.

rotation down the reaction coordinate to structure **22**, the last IRC structure that could be obtained. Geometry optimization of structure **22** gave minimum structure **16**, whose lowest vibrational frequency (133 cm^{-1}) corresponds exclusively to rotation of the $H_aC_1H_b$ methylene group. When this $H_aC_1H_b$ group is rotated in either direction by 10° increments and constrained, pathways from **16** to **12** are found on the (8,8)-CASSCF/6-31G* PES along which the energy decreases monotonically. In addition, transition structure **15** could be made to optimize to diradical **12** following small bi-directional rotations of the $H_aC_1H_b$ group of approximately 10°. The seven stationary points represented by structures **10** through **16** are the only ones located on the (8,8)CASSCF/6-31G* PES despite many attempts to locate a single transition structure between **10** and **11** (concerted reaction).

Thus it appears that two pathways exist between **10** and **11**, both involving diradical **12**. One of these pathways involves transition structure **13** and the other transition structure **15** (2.1 kcal/mol higher in energy), the latter one passing through structure **16**, likely an inflection point, on route to **12**. Presumably, the corresponding, slightly higher-energy, **10**→**15**→(**16**)→**12**→**14**→**11** pathway would not be expected to be "stereoselective". Unlike transition structure **13**, which has experienced substantial rotation of the C_1-C_2 bond in ascending

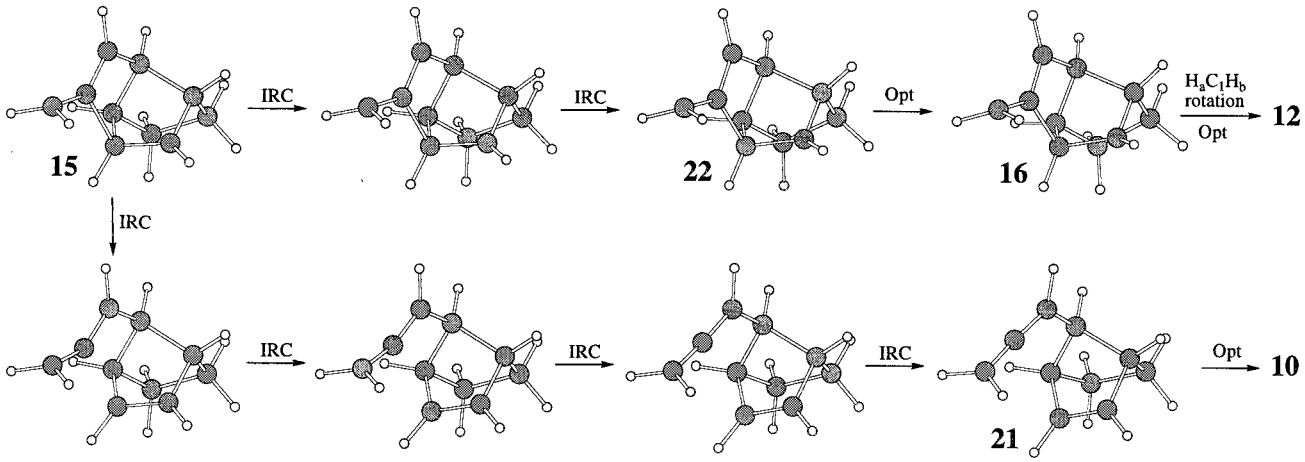

Figure 5. IRC structures for the rearrangement of **10** to **12**, involving transition structure **15** and intermediate **16**. Structures **21** and **22** represent the final points that could be obtained, on either side of the transition structure, by the IRC method. Intermediate IRC structures (i.e., unnumbered ones) represent equally spaced points between **15** and **21** as well as between **15** and **22**.

from **10** ($H_bC_1C_3H_c$ dihedral angle of **13** = 57.3°), transition structure **15** has experienced very little C_1-C_2 bond rotation ($H_bC_1C_3H_c$ dihedral angle of **15** = 88.4°). Thus, **15** should have little, if any, preference for the direction of rotation of its terminal $H_aC_1H_b$ group in the formation of diradical **12**.

These computational results are highly consistent with the 90% stereoselectivity observed experimentally in the Cope rearrangements of **7a** and **7b**: Most of the major products (e.g., (*E*)-**8** and (*Z*)-**9** in the case of **7a**) could result from a lower-energy stereospecific pathway resembling **10**→**13**→**12**→**14**→**11**, whereas the minor products (e.g., (*Z*)-**8** and (*E*)-**9** in the case of **7a**), and some of the major ones, could derive from a nonstereoselective higher energy pathway resembling **10**→**15**→(**16**)→**12**→**14**→**11**. The 68% stereoselectivity observed by Berson et al.[9] in the rearrangement of conformationally flexible **4** to triene **5** likely has a different explanation since the $H_aC_1H_b$ group of **1** is found to rotate little in proceeding along the PES to **17** or **18** ($H_bC_1C_3H_c$ dihedral angles = 78.2° and 76.0° respectively). The explanation suggested by the authors,[9] namely one involving equilibrating chair-form conformers of diradical **6**, likely accounts for a portion of the observed stereoselectivity. However, in light of the computational results on the rearrangement of **1**, in which a component of the reaction is found to be concerted in bypassing diradical intermediate **3**, it is likely that there is a stereospecific concerted component of the **4**→**5** rearrangement as well that does not involve diradical **6**.

Our computational results on the **10**→**11** rearrangement are found to differ from those obtained for the corresponding **1**→**2** allenyl Cope rearrangement[7] in two important respects. A single rate-determining transition structure **17** (cf. Figure 2) is implicated in the **1**→**2** rearrangement. As indicated above, it proceeds either to diradical intermediate **3** and then to transition structure **18** (cf. Figure 2) on the way to **2**, or through a **1**→**17**→**18**→**2** pathway which bypasses **3**. In the rearrangement of **10**, however, two separate rate-determining transition structures, **13** and **15,** are found, leading in one case to diradical **12** in a "stereoselective" sense (cf. Figures 3a and 4) and in the other to a "nonstereoselective" diradical **12** (cf. Figures 3b and 5).

The other important way in which the calculated pathways for **1**→**2** and **10**→**11** differ, concerns the way the allenyl group is utilized in each case. As shown in Table 1, the terminal C_1-C_2 bond in transition structure **17** has a computed bond length of 1.34 Å—close to normal for a C−C double bond—and the C_2-C_3 bond, a much longer one at 1.40 Å. By comparison, the corresponding C_1-C_2 and C_2-C_3 bond lengths in transition structure **13** are 1.37 and 1.36 Å, respectively. This difference is even more pronounced when transition structures **17** and **15** are compared. Structure **15** has C_1-C_2 and C_2-C_3 bond lengths of 1.41 and 1.34 Å, respectively, almost the exact reverse of those in **17**. Furthermore, whereas transition structures **17** and **18** do not appear to benefit much from allylic resonance delocalization (e.g., the respective $H_bC_1C_3H_c$ dihedral angles are 78.2° and 76.0°),[7] transition structures **13** and **14**, with $H_bC_1C_3H_c$ dihedral angles of 57.3° and 19.3° respectively, appear to benefit much more so, especially transition structure **14**. On the other hand, transition structure **15**, with a $H_bC_1C_3H_c$ dihedral angle of 88.4°, clearly does not exhibit allylic resonance stabilization.

These differences are also revealed by a comparison of the relevant active space orbitals[18] of (8,8)CASSCF/6-31G* transition structures **13**, **15**, and **17**, as shown in Figure 6. As Figure 6b clearly shows for transition structure **15**, the terminal allenyl π-bond plays a direct role in formation of the new σ-bond (orbital **I**) while the adjacent allenyl π-bond remains visibly intact (orbital **II**). (A similar, albeit less dramatic, effect is seen for transition structure **13** in Figure 6c.) However, as seen in Figure 6a, the forming σ-bond in transition structure **17** arises from the internal allenyl π-bond (orbital **I**); consequently it is the terminal allenyl π-bond that remains intact (orbital **II**). Correspondingly, an analysis of the calculated transition vectors for **13**, **15**, and **17** reveals a similar phenomenon. As shown in Figure 2, the transition vector for structure **17** is limited almost entirely to the motion of carbon atom 7, whereas in structures **13** and **15** the largest vector is associated with motion of the allenyl group that involves, in part, a significant stretching motion of the C_1-C_2 bond. Moreover, the magnitude of this vector is larger in transition structure **15** than it is in **13**, consistent with the longer C_1-C_2 bond length in **15**, relative to **13**. The active space orbitals depicted in Figure 6 also appear to demonstrate that among transition structures **13**, **15**, and **17**, only **13** exhibits significant allylic resonance delocalization (cf. orbital **II** of Figures 6c, 6b, and 6a, respectively).

Conclusions

The previously studied allenyl Cope rearrangement of 1,2,6-heptatriene (**1**) has been shown to proceed through one rate-

(18) A full set of complete active space molecular orbitals for transition structures **13**, **15**, and **17** are included with Supporting Information.

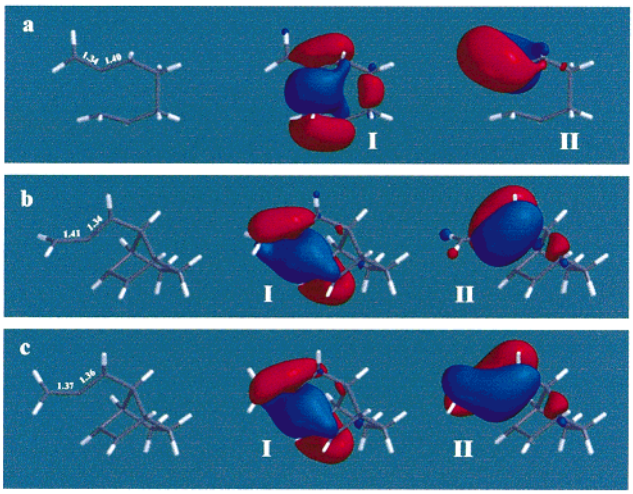

Figure 6. (a) Relevant active space orbitals for transition structure **17**, involved in the **1**→**2** rearrangement (bond lengths in Å): **I** involves the *internal* allenyl π-bond; **II** involves the *terminal* allenyl π-bond. (b) Relevant active space orbitals for transition structure **15**, involved in the **10**→**11** rearrangement: **I** involves the *terminal* allenyl π-bond; **II** involves the *internal* allenyl π-bond. (c) Relevant active space orbitals for transition structure **13**, involved in the **10**→**11** rearrangement: **I** involves the *terminal* allenyl π-bond; **II** involves primarily the *internal* allenyl π-bond.

determining transition state (**17**) that is involved in two distinct pathways, only one of which involves a diradical intermediate (**3**). Furthermore, the rearrangement of **1** does not involve direct participation of the terminal allenyl π-bond.[7] We have shown that the corresponding allenyl Cope rearrangement of *syn*-7-allenylnorbornene (**10**) is much more complicated, presumably as a consequence of the restriction in conformational mobility afforded the 1,2,6-heptatriene moiety in **10**. Its rearrangement proceeds through two pathways (cf. Figures 3a and 3b) that involve a common diradical intermediate (**12**) and that are distinguished by separate rate-determining transition states (**13** and **15**), a scenario consistent with the stereoselectivity observed in the rearrangement of the closely related allenylnorbornenes **7a** and **7b**.[10d] Most importantly, the rearrangement of **10** also involves direct participation of the terminal allenyl π-bond as represented by transition structures **13** and **15**, resulting in an augmented Cope process (cf. Figure 1c). The augmentation demonstrated by transition structure **15** is the more pronounced and remarkable. Apparently the overlap of the C_1-C_2 π-bond with the π-bond of the norbornene ring is so favorable that an accessible transition state (**15**), with virtually no allylic resonance stabilization, is observed to compete successfully with a slightly lower energy one (**13**), which can take advantage of a certain amount of allylic stabilization.

Acknowledgment. Support for this work from the M. J. Murdock Charitable Trust of Vancouver, Washington and Lewis & Clark College is gratefully acknowledged. We are also grateful to the National Science Foundation (Grant DUE−9750586) for providing funds for the purchase of several Silicon Graphics workstations used in the computations. We are especially indebted to Dr. David Hrovat of the University of Washington for his helpful advice during the course of this work and to Mr. Brian Arthur, System Administrator at Lewis & Clark College. We also thank Professor Kersey Black of Claremont McKenna College and Professor Alan Shusterman of Reed College for their assistance during the early stages of the work. Finally we thank former student Ingrid Susanto for encouraging us to undertake this study and for her early work on the project at lower levels of theory.

Supporting Information Available: (8,8)CASSCF/6-31G* optimized geometries and (8,8)CASPT2/6-31G* and (8,8)-CASSCF/6-31G* energies for structures **10**−**16**. A full set of complete active space molecular orbitals for transition structures **13**, **15**, and **17** (PDF). This material is available free of charge via the Internet at http://pubs.acs.org.

JA991838T